The Astrophysical Journal, 678:1109–1118, 2008 May 10

ACCRETION-POWERED STELLAR WINDS. II. NUMERICAL SOLUTIONS FOR STELLAR WIND TORQUES

Sean Matt[1] and Ralph E. Pudritz[2]
Received 2007 August 14; accepted 2008 January 17

ABSTRACT

In order to explain the slow rotation observed in a large fraction of accreting pre-main-sequence stars (CTTSs), we explore the role of stellar winds in torquing down the stars. For this mechanism to be effective, the stellar winds need to have relatively high outflow rates, and thus would likely be powered by the accretion process itself. Here, we use numerical magnetohydrodynamical simulations to compute detailed two-dimensional (axisymmetric) stellar wind solutions, in order to determine the spin-down torque on the star. We discuss wind driving mechanisms and then adopt a Parker-like (thermal pressure driven) wind, modified by rotation, magnetic fields, and enhanced mass-loss rate (relative to the Sun). We explore a range of parameters relevant for CTTSs, including variations in the stellar mass, radius, spin rate, surface magnetic field strength, mass-loss rate, and wind acceleration rate. We also consider both dipole and quadrupole magnetic field geometries. Our simulations indicate that the stellar wind torque is of sufficient magnitude to be important for spinning down a "typical" CTTS, for a mass-loss rate of $\sim 10^{-9}\ M_\odot\ \mathrm{yr}^{-1}$. The winds are wide-angle, self-collimated flows, as expected of magnetic rotator winds with moderately fast rotation. The cases with quadrupolar field produce a much weaker torque than for a dipole with the same surface field strength, demonstrating that magnetic geometry plays a fundamental role in determining the torque. Cases with varying wind acceleration rate show much smaller variations in the torque, suggesting that the details of the wind driving are less important. We use our computed results to fit a semianalytic formula for the effective Alfvén radius in the wind, as well as the torque. This allows for considerable predictive power, and is an improvement over existing approximations.

Subject headings: accretion, accretion disks — MHD — stars: magnetic fields — stars: pre–main-sequence — stars: rotation — stars: winds, outflows

1. INTRODUCTION

For more than half a century, the spin rates and the angular momentum evolution of stars have been topics of vigorous study. We know that stellar winds are responsible for the spinning down of late-type (later than F2) main-sequence stars (Parker 1958; Schatzman 1962; Kraft 1967; Skumanich 1972; Soderblom 1983; Kawaler 1988; MacGregor & Brenner 1991; Barnes & Sofia 1996; Bouvier et al. 1997). There is still progress to be made on main-sequence star spins (Barnes 2003), but perhaps the largest open questions remain at the pre-main-sequence phase, which determines the "initial conditions" for the spin histories of stars.

By the time intermediate/low-mass ($\lesssim 2\ M_\odot$) pre-main-sequence stars become optically visible (T Tauri stars; TTSs), they already have ages around 10^5–10^6 yr. A large fraction of TTSs (called classical TTSs; CTTSs) are observed to actively accrete material from a disk at a rate within a wide range of $\sim 10^{-8}\ M_\odot\ \mathrm{yr}^{-1}$ (e.g., Johns-Krull & Gafford 2002). At this rate, the angular momentum accreted from the orbiting disk should spin up the stars to a substantial fraction of breakup speed in a short amount of time (comparable to their ages). The fact that the stars are also still contracting (e.g., Rebull et al. 2002), and that they presumably were accreting at much higher rates before they became optically visible, further adds to the expectation of fast rotation.

Large data sets for the spins of TTSs in star formation regions and clusters of different ages (see Rebull et al. [2004] for a compilation) show that approximately half of the stars are rotating rapidly and do seem to spin up as expected as they approach zero-age main sequence (Vogel & Kuhi 1981; Bouvier et al. 1997; Rebull et al. 2004; Herbst et al. 2007). However, the surprise is that the other approximately half of TTSs exhibit much slower rotation rates (∼10% of breakup speed) at all ages. Recent studies have shown a correlation between slow rotation and the presence of an accretion disk (see especially Cieza & Baliber 2007), although this idea has been controversial in the past (e.g., Stassun et al. 1999, 2001; Herbst et al. 2000, 2002). This is still an open issue, but it is clear than an efficient angular momentum loss or regulation mechanism is operating for the slow rotators.

Although alternative ideas have been proposed since (Königl 1991; Shu et al. 1994; see Matt & Pudritz [2008a] for a history), Hartmann & Stauffer (1989) offered the first potential explanation for the slow rotators, namely that massive stellar winds may be responsible for carrying off substantial angular momentum (see also Tout & Pringle 1992). In Matt & Pudritz (2005a; hereafter Paper I), we extended this idea to consider the effects of the magnetic interaction between the star and disk, and we used a one-dimensional scaling from the solar wind angular momentum loss to estimate the torque for TTSs. The scaling suggested that, for an observationally constrained dipole magnetic field strength of 200 G (e.g., Johns-Krull et al. 1999; Bouvier et al. 2007; Johns-Krull 2007a, 2007b; Smirnov et al. 2003a; Yang et al. 2007), it might indeed be possible for the stellar wind to extract enough angular momentum to explain the slow rotators. For stellar winds to balance the accreted angular momentum, the wind outflow rate needs to be a substantial fraction of the accretion rate. In Paper I, we suggested that this is possible, if a fraction of the energy liberated by the accretion process actually powers the stellar wind.

The pre-main-sequence phase is, in fact, marked by powerful outflows (Reipurth & Bally 2001). In the most powerful sources, due to the large linear momenta of the outflows (Königl & Pudritz 2000), the X-ray luminosities (Decampli 1981), and possible

[1] Department of Astronomy, University of Virginia, P.O. Box 400325, Charlottesville, VA 22904-4325; seanmatt@virginia.edu.
[2] Physics and Astronomy Department, McMaster University, Hamilton, ON L8S 4M1, Canada; pudritz@physics.mcmaster.ca.

detection of rotation (Bacciotti et al. 2002; Anderson et al. 2003; Coffey et al. 2004, 2007; Ferreira et al. 2006), it appears that most of the flow arises from the accretion disk rather than the star. It is not clear what fraction of the total outflow may actually originate from the star, and thus how powerful the stellar winds are compared to main-sequence phase winds or to their accretion rates.

There is some observational evidence for powerful stellar winds from CTTSs, as distinguished from inner disk winds. In particular, Edwards et al. (2003, 2006) observed the He I λ10830 line in 39 CTTSs and saw several cases with a broad, deep, blue-shifted absorption, indicating outflow velocities of typically a few hundred, and up to $\sim$400 km s^{-1}. They concluded that this feature is best interpreted as arising in an optically thick stellar wind (see also Dupree et al. 2005). They also suggested that the winds may be accretion powered, since the wind signatures are most prevalent in the stars with highest accretion rates and absent in nonaccreting systems. Subsequent modeling of the He I λ10830 line by Kwan et al. (2007) indicates that approximately half of these CTTSs show evidence for a powerful stellar wind. Furthermore, Kurosawa et al. (2006) modeled the Hα emission line in these systems and suggested that a stellar wind component could most naturally explain the profiles observed in $\sim$7% of the stars in a sample compiled by Reipurth et al. (1996).

There already exists some theoretical work on stellar winds, specifically from pre-main-sequence stars, with a focus on the wind driving mechanism (Decampli 1981; Hartmann et al. 1982, 1990) or the collimation of the winds (Fendt et al. 1995; Fendt & Camenzind 1996; Bogovalov & Tsinganos 2001; Sauty et al. 2002). These do not discuss the expected angular momentum outflow rates, however. The works that do calculate stellar wind torques for pre-main-sequence stars (Hartmann & MacGregor 1982; Mestel 1984; Hartmann & Stauffer 1989; Tout & Pringle 1992; Paatz & Camenzind 1996; Paper I) are either based on a one-dimensional formulation and/or have made a priori simplifying assumptions regarding the stellar magnetic field structure, wind flow speed, and latitudinal dependence of the wind. Calculating the stellar wind torque reliably is a complex, multidimensional problem, and more work is needed to develop the stellar wind theory further.

The primary goal of this paper therefore, is to take the next major step in developing the accretion-powered stellar wind picture by rigorously computing the steady state solutions of winds from spinning magnetized stars. We carry out a parameter study to provide a range of possible solutions that are expected to characterize accretion-powered stellar winds. Where possible, we compare our results to analytic magnetohydrodynamic (MHD) stellar wind theory. In a companion paper, we will use these solutions to compare the stellar wind torques and wind driving power with the torque and energy deposition expected to arise from the interaction of the star with its accretion disk.

In the following section (§ 2.1), we give a brief introduction to basic stellar wind theory. This provides the motivation for using a numerical approach and sets the stage for comparing our numerical results with the analytic theory. Section 2.2 contains a discussion of our adopted wind driving mechanism. We describe our numerical method for obtaining solutions in § 3, and present the results in § 4. Section 5 contains a semianalytic formulation for the torque and a comparison to previous theory.

2. MAGNETIZED STELLAR WINDS: NEEDED BACKGROUND

2.1. *Magnetic Stellar Wind Theory*

Standard MHD wind theory (i.e., magnetic rotator theory), following Weber & Davis (1967), characterizes a steady state flow of plasma along a magnetic field line that is anchored to a rotating object, which we will hereafter take to be a star. One of the key results is that the angular momentum outflow rate per unit mass loss is given very simply as (see, e.g., Weber & Davis 1967; Mestel 1968; Michel 1969)

$$l = \Omega_* r_{\rm A}^2, \tag{1}$$

where Ω_* is the angular rotation rate of the star, and $r_{\rm A}$ is the cylindrical radius at which the outflow speed equals the local magnetic Alfvén speed,

$$v_{\rm A} \equiv \frac{B_p}{\sqrt{4\pi\rho}}, \tag{2}$$

where ρ is the local mass density and B_p is the strength of the poloidal magnetic field, $B_p = (B_r^2 + B_z^2)^{1/2}$, in cylindrical (r, ϕ, z) coordinates. Equation (1) indicates that the quantity of angular momentum carried in the wind is *as if* the wind material is corotating out to $r_{\rm A}$ and conserves its angular momentum thereafter. Thus, $r_{\rm A}$ is often referred to as the magnetic "lever arm." In reality, the azimuthal velocity of the wind, v_ϕ, is a smooth (i.e., differentiable) function of radius, and the difference between $v_\phi r$ and l at all radii equals the torque transmitted by azimuthally twisted magnetic field lines.

By integrating the mass flux times l over any surface enclosing the star, one obtains an expression for the total angular momentum outflow rate and, by Newton's third law, the torque on the star:

$$\tau_w = -\dot{M}_w \Omega_* \left\langle r_{\rm A}^2 \right\rangle, \tag{3}$$

where $\dot{M}_w$ is the integrated wind mass-loss rate. Since the value of $r_{\rm A}$ will generally not be the same along each field line, equation (3) defines the quantity $\langle r_{\rm A}^2 \rangle$, which is the mass-loss-weighted average of $r_{\rm A}^2$ (suggested by Washimi & Shibata 1993). Hereafter, we will simply refer to this average as $r_{\rm A} \equiv \langle r_{\rm A}^2 \rangle^{1/2}$.

The difficulty now lies in calculating $r_{\rm A}$. The lever arm length clearly depends on the stellar surface field strength (B_*), stellar radius (R_*), and $\dot{M}_w$ because these directly affect Alfvén condition. But it also depends on the flow speed and field structure, which are not possible to determine a priori in the wind. The flow speed is influenced by the thermal energy in the wind as well as rotation. There exist two different regimes (Belcher & MacGregor 1976): the fast magnetic rotator regime, where the flow speed is mostly determined by magnetorotational effects; and the slow magnetic rotator, where the flow speed is solely determined by the wind driving. The field structure in the wind, even though the geometry may be known at the stellar surface, is determined by the self-consistent interaction between the wind and rotating magnetic field and thus is a function of all parameters. Therefore one can only calculate $r_{\rm A}$ by making a priori assumptions about the field structure and/or flow speed (Weber & Davis 1967; Mestel 1968, 1984; Okamoto 1974; Mestel & Spruit 1987; Kawaler 1988) or by using iterative techniques (or numerical simulations; Pneuman & Kopp 1971; Sakurai 1985; Washimi & Shibata 1993; Keppens & Goedbloed 2000; Matt & Balick 2004).

All of these methods are complementary. The analytical work, in which the field structure is guessed, produces a predictive formulation of the stellar wind torque (e.g., Kawaler 1988). However, the formulation of the field structure usually introduces more parameters (such as a power-law index for the magnetic field), so that almost any result can be obtained by adjusting

these. Furthermore, the field structure in the analytic models has no explicit dependence on (for example) Ω_*, which is exhibited in numerical simulations (e.g., Matt & Balick 2004). The numerical simulation technique has the advantage of calculating the field structure and flow speed self-consistently. However, a single simulation does not predict the dependence of r_A on parameters, and to date, not enough parameter space has been explored. Thus, to date, there exists no formulation for the stellar wind torque that convincingly applies over a wide range of conditions (e.g., over a range of B_*, $\dot{M}_w$, and Ω_*).

In this paper we will use two-dimensional (axisymmetric) MHD simulations to calculate the torque and corresponding value of r_A. This will allow us to check the estimate for r_A of Paper I (and previous works). In addition, we will carry out a parameter study to determine the dependence of the stellar wind torque on parameters, over a range of conditions appropriate for TTSs, and compare this with the predictions of analytic theory.

2.2. *Wind Driving Mechanism*

It is not known what drives winds from TTSs. These stars have active coronae (Feigelson & Montmerle 1999; Stassun et al. 2004; Favata et al. 2005), and it thus seems a reasonable assumption that they also drive solar-like coronal winds in which thermal pressure plays a significant role in the wind acceleration. Based on a calculation from Bisnovatyi-Kogan & Lamzin (1977), Decampli (1981) concluded that, in order for the wind emission to be consistent with the X-ray observations, the mass-loss rate of a TTS coronal wind must be less than $\sim 10^{-9}\ M_\odot\ \mathrm{yr}^{-1}$. Furthermore, Dupree et al. (2005) found evidence for a stellar wind with a coronal temperature in the CTTS TW Hya (although this conclusion has been challenged by Johns-Krull & Herczeg 2007).

The assumption of thermal pressure driving is a simplification, even for the solar wind. It is known that a major factor in driving the solar wind is Alfvén wave momentum and energy deposition. Two important recent studies have done self-consistent analyses of the combined problem of both solar wind heating and acceleration (Suzuki & Inutsuka 2006; Cranmer et al. 2007). The first paper shows that low-frequency, transverse motions of open field lines at the photosphere leads to transonic solar winds for superradial expansion of the wind cross section. If the amplitude of these transverse photospheric motions exceeds 0.7 km s^{-1}, fast winds are produced and the dissipation of wave energy heats the atmosphere to a million degrees. The results are sensitive to the amplitude of the velocity perturbations, and the simulations show that the solar wind virtually disappears for amplitudes $\leq$0.3 km s^{-1}. These numerical simulations also show that Alfvén wave pressure dominates the gas pressure in the solar acceleration region ($1.5\ R_\odot \leq R \leq 10\ R_\odot$). The second paper shows similar results. This work shows that there are three key parameters that control wind heating and acceleration: the flux of acoustic power injected at the photosphere, the Alfvén wave amplitude there, and the Alfvén wave correlation length (characterizing wave damping through turbulence) at the photosphere.

Our primary goal here is to evaluate the angular momentum transported away from the star by the stellar wind. Thus, in this work, we do not discuss the thermodynamic properties of the wind and instead focus on the angular momentum transport. Fortunately, this torque does not much depend on what drives the wind. Rather, the torque depends primarily on the stellar magnetic field, rotation rate, radius, $\dot{M}_w$, and the wind velocity. As long as "something" accelerates the wind to speeds similar to what we see in our simulations, the torque we calculate will be approximately correct.

We expect that the Alfvén waves in accreting TTS winds will have a significant, if not dominant, contribution to both the acceleration and heating of their winds. These waves will be launched along the open field lines that originate from the TTS photosphere at latitudes comparable to those that harbor field lines carrying the accretion flow onto the star. The irregular accretion flow should generate very large (i.e., much larger than acoustic motions in the solar photosphere) acoustical transverse motions in the TTS photosphere as it impinges on the star. These large amplitude perturbations, generated by the accretion flow itself, may be the ultimate driver for the Alfvén wave flux that drives our proposed accretion-powered stellar wind.

Note that the driving force can be parameterized as being proportional to $-\nabla\xi$ (where ξ is the wave energy density; Decampli 1981). This has the same functional form as the thermal pressure force ($-\nabla P$) used in our simulations. Several authors (e.g., Hartmann & MacGregor 1980; Decampli 1981; Holzer et al. 1983; Suzuki 2007) computed velocity profiles for cool ($\sim 10^4$ K) Alfvén wave-driven winds. These works exhibit wind velocity profiles that are similar to what is expected from thermal pressure driving of hotter winds. Therefore, we can think of thermal pressure driving as a proxy for some other driving mechanism. Also, it will be important to have these solutions to compare with future work that includes different driving mechanisms.

In this paper, we restrict ourselves to mass-loss rates of $\dot{M}_w < 2\times 10^{-9}\ M_\odot\ \mathrm{yr}^{-1}$. As justified above, we adopt a Parker-like (Parker 1958) coronal wind driving mechanism, modified by magnetic fields, stellar rotation, and an enhanced mass-loss rate (relative to the Sun). As the nature (e.g., temperature) of TTS stellar winds is not well known, our detailed solutions of coronal winds will enable us to look at the expected radiative properties, a posteriori, allowing for further constraints on real systems. We will show in a forthcoming paper (and see Matt & Pudritz 2007) that the expected emission from the simulated winds presented here rules out thermal pressure driving at a substantially lower mass-loss rate than the limit of Decampli (1981).

3. NUMERICAL SIMULATION METHOD

We calculate solutions of steady state winds from isolated stars (no accretion disk), using the finite-difference MHD code of Matt & Balick (2004); the reader will find further details there[3] (and references therein). Assuming axisymmetry and using a cylindrical (r, ϕ, z) coordinate system, the code employs a two-step Lax-Wendroff scheme (Richtmyer & Morton 1967) to solve the following time-dependent, ideal MHD equations:

$$\frac{\partial \rho}{\partial t} = -\nabla\cdot(\rho \boldsymbol{v}), \tag{4}$$

$$\frac{\partial(\rho \boldsymbol{v})}{\partial t} = -\rho(\boldsymbol{v}\cdot\nabla)\boldsymbol{v} - \boldsymbol{v}[\nabla\cdot(\rho\boldsymbol{v})] - \nabla P - \frac{GM_*\rho}{(\boldsymbol{r}^2+\boldsymbol{z}^2)}\hat{\boldsymbol{R}} + \frac{1}{c}(\boldsymbol{J}\times\boldsymbol{B}), \tag{5}$$

$$\frac{\partial e}{\partial t} = -\nabla\cdot[\boldsymbol{v}(e+P)] - \left[\frac{GM_*\rho}{(\boldsymbol{r}^2+\boldsymbol{z}^2)}\hat{\boldsymbol{R}}\right]\cdot\boldsymbol{v} + \boldsymbol{J}\cdot\boldsymbol{E}, \tag{6}$$

$$\frac{\partial \boldsymbol{B}}{\partial t} = -c(\nabla\times\boldsymbol{E}), \tag{7}$$

[3] Matt & Balick (2004) ran cases with isotropic hydrodynamic variables at the base of the wind and also cases with enhanced polar winds. Here we only consider the isotropic case.

and uses

$$\boldsymbol{E} = -\frac{1}{c}(\boldsymbol{v}\times\boldsymbol{B}), \tag{8}$$

$$\boldsymbol{J} = \frac{c}{4\pi}(\nabla\times\boldsymbol{B}), \tag{9}$$

$$e = \frac{1}{2}\rho v^2 + \frac{P}{\gamma-1}, \tag{10}$$

where ρ is the density, $\boldsymbol{v}$ the velocity, P the gas pressure, G Newton's gravitational constant, M_* the stellar mass, R the spherical distance from the center of the star ($R^2 = r^2 + z^2$), e the internal energy density, $\boldsymbol{B}$ the magnetic field, $\boldsymbol{J}$ the volume current, $\boldsymbol{E}$ the electric field, c the speed of light, and γ the ratio of specific heats.

To obtain steady state wind solutions, we follow the method of Matt & Balick (2004), which is also similar to that employed by Washimi & Shibata (1993) and Keppens & Goedbloed (1999). It involves initializing the computational grid with a spherically symmetric, isothermal Parker wind solution (Parker 1958), plus force-free dipole (and sometimes quadrupole) magnetic field. When the simulation begins, the wind solution changes from the initial state due to the presence of the magnetic field, the rotation of the star, and the polytropic equation of state ($P \propto \rho^\gamma$). The simulations run until the system relaxes into a steady state (within a small tolerance) MHD wind solution. The code uses nested computational grids so that the wind can be easily followed to large distances (several tens to hundreds of R_*).

This method results in a steady state solution for the wind that is determined solely by the boundary conditions held fixed at the base of the stellar corona (the "stellar surface"). In order to capture the appropriate physics within the framework of a finite difference scheme, we employ a four-layer boundary for the star, on which the various physical quantities are set as follows. We consider the spherical location $R = 30$, in units of the grid spacing, to be the surface of the star. For all grid points such that $R \leq 34.5$, the poloidal velocity is forced to be parallel with the poloidal magnetic field ($v_p \parallel B_p$, where the poloidal component is defined as the vector component in the r-z plane). Where $R \leq 33.5$, ρ and P are held constant (in time) at their initial values. For $R \leq 32.5$, v_p is held at zero, while v_ϕ is held at corotation with the star. For $R \leq 31.5$, B_p field is held at its initial, dipolar value, while B_ϕ is set so that there is no poloidal electric current at that layer (which gives it a dependence on the conditions in the next outer layer, $31.5 < R \leq 32.5$).

These boundary conditions properly capture the behavior of a wind accelerated from the surface of a rotating magnetized star, as follows. There is a layer on the stellar boundary ($R > 32.5$), outside of which the velocity not fixed, but is allowed to vary in time. In this way, the wind speed and direction is not specified, but is determined by the code in response to all of the forces. By holding P fixed at its initial value for all $R \leq 33.5$, we constrain the pressure gradient force (thermal driving) at the base of the wind to be constant in time. In addition, holding the density fixed at $R \leq 33.5$ allows the region from which the wind flows to be instantly replenished with plasma. Thus, the base of the wind maintains a constant temperature and density, regardless of how fast or slow the wind flows away from that region. The existence of a layer in which $v_p = 0$ and B_p can evolve (namely, at $31.5 < R \leq 32.5$) allows B_p (and v_p) to reach a value that is self-consistently determined by the balance of magnetic and inertial forces. We set the poloidal velocity parallel to the poloidal magnetic field for the next two outer layers, to ensure a smooth transition from the region of pure dipole field and zero velocity to that with a perturbed field and outflow. Setting B_ϕ so that the poloidal electric current is zero inside some radius ensures that the field behaves as if anchored in a rotating conductor (the surface of the star). Also, this ensures that B_ϕ evolves appropriately outside the anchored layer according to the interaction with the wind plasma.

The key physical parameters can be represented by the characteristic speeds of the input physics, namely the sound speed at the base of the corona, c_s, the escape speed from the surface of the star, $v_{\rm esc}$, the rotation speed of the star, and the Alfvén speed at the base of the wind. We specify the ratio of $c_s/v_{\rm esc}$ as our parameter, rather than the sound speed alone. This seems the most reasonable, since the temperature of a thermally driven wind is regulated somewhat by the interplay between the thermal energy input and the expansion of the corona (the wind) against gravity. To first order, a hotter wind expands more rapidly against gravity, allowing less time for the gas to heat, and a cooler wind expands more slowly, allowing more time to heat. Once the value of the stellar mass and radius is specified, the ratio of $c_s/v_{\rm esc}$ determines the temperature held fixed on the stellar boundary, as described above. The wind plasma is characterized by a polytropic equation of state, and so γ is also a parameter. We parameterize the stellar rotation rate as the fraction of breakup speed,

$$f \equiv \Omega_* R_*^{3/2}(GM_*)^{-1/2}. \tag{11}$$

The Alfvén speed is determined by the magnetic field strength and coronal density. Rather than taking the Alfvén speed as a key parameter, we specify the field strength at the equator of the star (B_*) as our parameter, in order to connect the simulations as much as possible to observationally constrained quantities. For the same reason, we specify $\dot{M}_w$ as a parameter, rather than the coronal density. In the simulations, we must specify the base density, ρ_*, to be held fixed on the stellar boundary, and the value of $\dot{M}_w$ in the steady state wind is not solely determined by ρ_*. For example, the rotation of the star can enhance $\dot{M}_w$ via magneto-centrifugal flinging, and a strong magnetic field can decrease $\dot{M}_w$ by inhibiting flow from a region near the equator that remains magnetically closed (the "dead zone"). In other words, $\dot{M}_w$ is not an a priori tunable parameter; rather, it is a result of the simulations. Therefore, to treat $\dot{M}_w$ as our tunable parameter, we adopt an iterative approach. This entails first running a given simulation with a guess for ρ_*, checking the resulting value of $\dot{M}_w$, and then adjusting ρ_* and rerunning the simulation. We iterate until the desired value of $\dot{M}_w$ is achieved (within a tolerance of 2%). This typically required 2–4 iterations, so the ability to treat $\dot{M}_w$ as a chosen parameter comes at a substantial cost.

4. STELLAR WIND SOLUTIONS

4.1. *The Fiducial Case*

We start by presenting the results of our stellar wind simulation for parameters with values that represent a "typical" TTS and follow the fiducial values of Paper I and Matt & Pudritz (2005b). Table 1 lists the fiducial parameters. We consider a low-mass pre-main-sequence star, with a surface escape speed of $v_{\rm esc} \approx 309$ km s^{-1}. A dipole magnetic field strength of 200 G is consistent with 3 σ upper limits (Johns-Krull et al. 1999; Smirnov et al. 2004, 2003b) or marginal detection (Smirnov et al. 2003a; Yang et al. 2007) of the longitudinal magnetic field measured for CTTSs. We seek primarily to understand the slow rotators, for which a rotation rate of 10% of breakup is appropriate. In Paper I,

TABLE 1
FIDUCIAL STELLAR WIND PARAMETERS

Parameter	Value
M_*	0.5 $M_\odot$
R_*	2.0 $R_\odot$
B_* (dipole)	200 G
f	0.1
$\dot{M}_w$[a]	1.9×10^{-9} $M_\odot$ yr^{-1}
$c_s/v_{\rm esc}$	0.222
γ	1.05

[a] In order to treat $\dot{M}_w$ as a parameter in the simulations, our method is to adjust the mass density at the base of the wind until the desired $\dot{M}_w$ is achieved in the steady state.

we estimated that an accretion-powered stellar wind for a TTS might have $\dot{M}_w \approx 1.9 \times 10^{-9}$ $M_\odot$ yr^{-1}, so we use this as our fiducial value.

In a thermally driven wind, the coronal sound speed should be comparable to the escape speed, and we use $c_s/v_{\rm esc} = 0.222$ as our fiducial value. This value gives wind speeds that are appropriate in the solar case. The choice of polytropic index γ is also important. At large distances ($\sim$AU) from the Sun, the solar wind plasma is well characterized by an effective γ between approximately 1.5 and 5/3 (Feldman et al. 1998; Krasnopolsky 2000). However, in the region where the wind is accelerated (within a few solar radii), thermal conduction and other heating and cooling effects play a role (e.g., Cranmer et al. 2007), resulting in an effective γ closer to unity (isothermal). Our fiducial value of $\gamma = 1.05$ was used by Washimi & Shibata (1993) and Matt & Balick (2004) for solar-like winds. This nearly isothermal value of γ approximates the thermodynamics of a gas with a true value of $\gamma = 5/3$ that is heated as it expands.

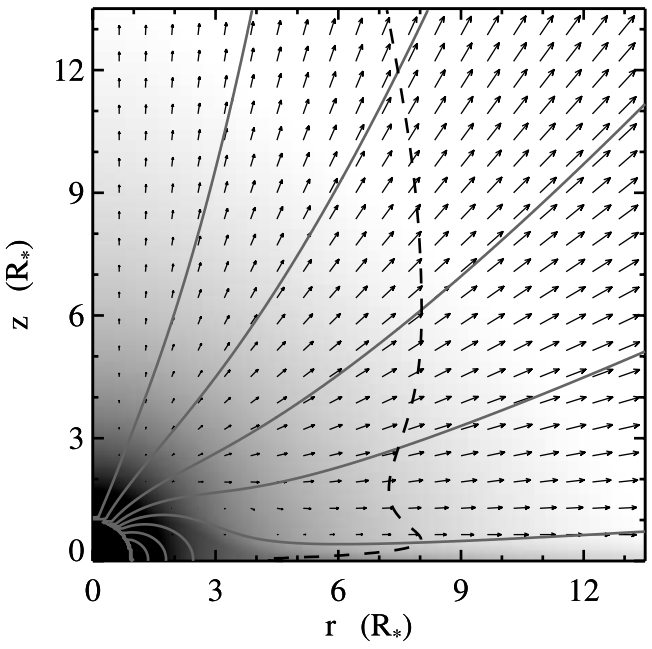

FIG. 1.—Fiducial case: grey scale of log density, velocity vectors, and magnetic field lines illustrate the structure of the steady state wind solution (see Table 1). The dashed line represents the Alfvén surface, where the wind speed equals the local Alfvén speed. The rotation axis is vertical, and the longest vector corresponds to 160 km s^{-1}. Black corresponds to a density above 5.3×10^{-13} g cm^{-3} and white to a density below 2.6×10^{-16} g cm^{-3}.

TABLE 2
STELLAR WIND TORQUES AND LEVER ARM LENGTHS

Case	ρ_* (10^{-11} g cm^{-3})	$\dot{M}_w$ (10^{-9} $M_\odot$ yr^{-1})	τ_w (10^{36} erg)	$\langle r_{\rm A}^2 \rangle^{1/2}$ (R_*)
Fiducial	3.67	1.89	1.77	6.97
$f = 0.004$	7.62	1.86	0.0972	8.33
$f = 0.2$	1.36	1.87	2.82	6.26
$f = 0.05$	6.01	1.88	1.06	7.65
$B_* = 400$ G	3.67	1.86	3.27	9.55
$B_* = 2$ kG	3.67	1.92	13.8	19.3
1 kG quad.	2.92	1.87	1.37	6.17
2 kG quad.	4.38	1.93	2.11	7.53
Low $\dot{M}_w$	0.377	0.187	0.500	11.8
Very low $\dot{M}_w$	0.0755	0.0378	0.204	16.7
$R_* = 1.5$ $R_\odot$	5.71	1.86	1.10	5.96
$R_* = 3$ $R_\odot$	1.99	1.89	3.43	8.75
$M_* = 0.25$ $M_\odot$	5.06	1.91	1.47	7.52
$M_* = 1$ $M_\odot$	2.59	1.88	2.11	6.42
$c_s/v_{\rm esc} = 0.245$	0.773	1.87	1.59	6.64
$c_s/v_{\rm esc} = 0.192$	55.4	1.89	1.91	7.23
$\gamma = 1.10$	11.1	1.87	2.19	7.79

Figure 1 shows the result of our fiducial case simulation, which illustrates the steady state wind solution. The nonspherical shape of the Alfvén surface (which eventually crosses the rotation axis at larger radii than shown) is mainly due to magneto-rotational effects in the wind (see Washimi & Shibata 1993; Matt & Balick 2004). This demonstrates that the fiducial TTS wind exists in the thermocentrifugal regime where thermal and magnetocentrifugal effects are of similar importance for accelerating the wind (Sakurai 1985; Washimi & Shibata 1993). These winds are self-collimated, while still exhibiting substantial flow at all latitudes.

From the simulation, we calculate $\dot{M}_w$ and the total angular momentum outflow rate, τ_w, as described by Matt & Balick (2004). Then, using equation (3), we calculate the effective lever arm length, $r_{\rm A} \equiv \langle r_{\rm A}^2 \rangle^{1/2}$. These results are listed in the first row of Table 2, where we also list the coronal base density ρ_* that we iteratively chose to give the desired value of $\dot{M}_w$.

The wind base density of $\sim 10^{-11}$ gm cm^{-3} is 5 orders of magnitude larger than required for simple solar wind models (e.g., Washimi & Shibata 1993). This is expected, since the fiducial $\dot{M}_w$ is 5 orders of magnitude higher than the solar value, and the wind speeds are comparable.

The fiducial stellar wind torque of $\approx 1.8 \times 10^{36}$ erg is capable of balancing the spin-up torque from accretion at a rate of 4.4×10^{-9} $M_\odot$ yr^{-1}. The basic conclusion here is that the stellar wind torque for the fiducial case is of the right magnitude to be important for spinning down the star, as required by the accretion-powered stellar wind scenario. We chose our fiducial parameters to compare with the estimate of Paper I that $r_{\rm A}/R_* \approx 12.2$.[4] We can see that their estimate, based on scaling of one-dimensional wind theory from solar values, was a 75% overestimate of $r_{\rm A}$. We will identify the reasons for this in § 4.2.1.

4.2. *Parameter Study*

To establish the dependence of $r_{\rm A}$ on parameters and to calculate wind solutions that are applicable to a wide range of conditions that are observed or often assumed for TTSs, we carried

[4] Paper I actually quotes a value of $r_{\rm A}/R_* = 15$, but our definition differs slightly here (compare eq. [3] here with eq. [2] of Paper I), so the lever arm length corresponds to 12.2 R_* here.

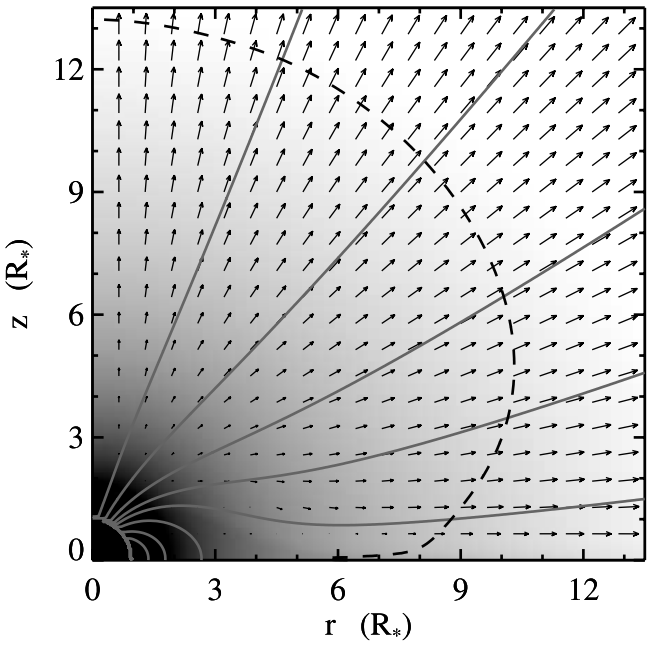

FIG. 2.—Same as Fig. 1, but for the $f = 0.004$ (similar to solar) case. The maximum velocity vector corresponds to 95 km s^{-1}.

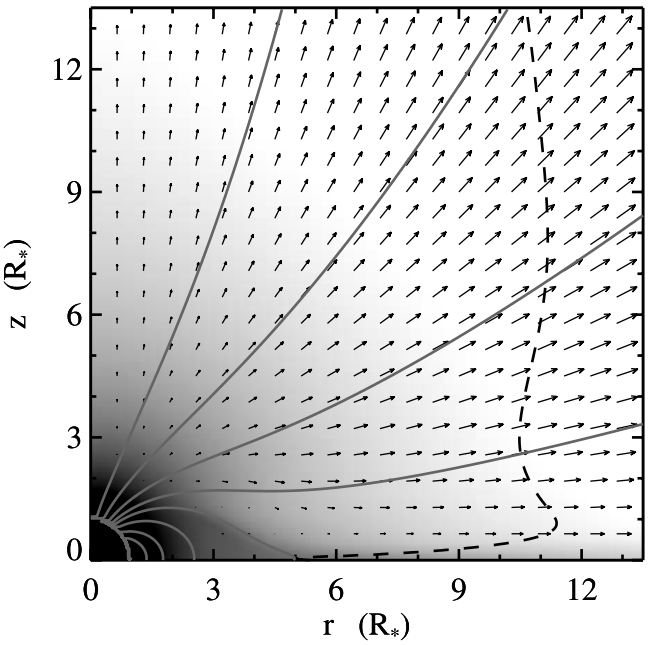

FIG. 3.—Same as Fig. 1, but for the $B_* = 400$ G dipole case. The maximum velocity vector corresponds to 190 km s^{-1}.

out a limited parameter study with our simulations. The results are listed in Table 2, and we briefly discuss each case below. The first column in the table lists the value of the parameter that is changed relative to the fiducial case. For each case, all other parameters are identical to the fiducial case. Note that since we consider $\dot{M}_w$ as a key parameter, the value of ρ_* varies from case to case.

4.2.1. *Spin Rate*

As with the fiducial case, all but one simulation in our parameter study lie in a regime that is near the boundary between slow and fast magnetic rotators. The one exception is a case with a fractional rotation rate equal to the solar value of $f = 0.004$, which represents a slow magnetic rotator. Figure 2 illustrates the structure of the steady state wind solution for this case in the same format as the previous figure. A comparison between the two figures reveals that rotation indeed influences the detailed structure of the velocity field and the magnetic field in the wind, which manifests itself as a difference in the shape of the Alfvén surface. All else being equal, the effect of faster rotation is to reduce the effective lever arm length, as evident in Table 2 (see also Sakurai 1985; Washimi & Shibata 1993). Although the qualitative effect of rotation on the shape of the Alfvén surface was anticipated in analytic theory (e.g., Belcher & MacGregor 1976), this effect is not properly included in any existing analytic formulation for calculating the torque. This is a primary reason that numerical simulations are required to convincingly calculate the self-consistent wind solution, especially when considering winds that exist near the boundary between slow and fast magnetic rotators. The effect of rotation on r_A was not considered in the estimate of Paper I and accounts for approximately 30% of their overestimate of r_A.

As described in Matt & Balick (2004), a given simulation can be scaled to other systems with the same characteristic velocity ratios, so that the resulting value of r_A/R_* is valid for a family of solutions. The simulation with $f = 0.004$ scales to a solution very similar to the solar wind with $R_* = 1\ R_\odot$, $M_* = 1\ M_\odot$, $\dot{M}_w = 1.3 \times 10^{-14}\ M_\odot$ yr^{-1}, $B_* = 1.5$ G, and all speeds are increased by a factor of 2. Thus, for these parameters, this simulation predicts a lever arm length of 8.33 $R_\odot$ for the case of the solar wind, and $\tau_w = 6.8 \times 10^{29}$ erg. This torque is consistent with the numerical results of Washimi & Sakurai (1993) but a factor of a few times smaller than observationally determined values (Li 1999). To obtain the observed solar torque, corresponding to $r_A = 12.2\ R_\odot$, the simulation would require (e.g.) a substantially stronger magnetic field than 1 G. This was also suggested by Li (1999), and our simulations corroborate that suggestion. As the estimate in Paper I assumed the canonical value of $B_* \approx 1$ G for the Sun, this accounts for most of the discrepancy between our simulation results and the Paper I estimate of r_A.

To capture a range of spins appropriate for the TTS "slow rotators," we also ran cases with spin rates of twice and half of the fiducial spin rate. The results of these simulations are listed in the third and fourth rows of Table 2.

4.2.2. *Dipole Field Strength*

Measurements for the mean $|B_*|$ exist for a number of TTSs (e.g., Johns-Krull 2007b). These results show a remarkably consistent field strength for all stars of around 2 kG. Measurements of the longitudinal field (which limits the global, dipole component) exist only for a handful of accreting stars (Bouvier et al. 2007; Johns-Krull 2007a). These measurements suggest the dipole component is no greater than 200 G (although larger values would be allowed for special viewing geometries). Given the small number of measurements, it is still relevant to consider stronger dipole field strengths. Thus we have run cases with $B_* =$ 400 and 2 kG.

Figure 3 illustrates the wind solution for the case with $B_* =$ 400 G, and the results of both cases are listed in Table 2. It is clear that the strength of the field has a strong influence on the stellar wind torque.

4.2.3. *Surface Field Geometry*

The fact that TTSs have a mean field of $|B_*| \sim 2$ kG with a much weaker dipole component indicates that the stellar surface field is dominated by higher order multipole fields. Therefore, it may be important for future work to include much more structured

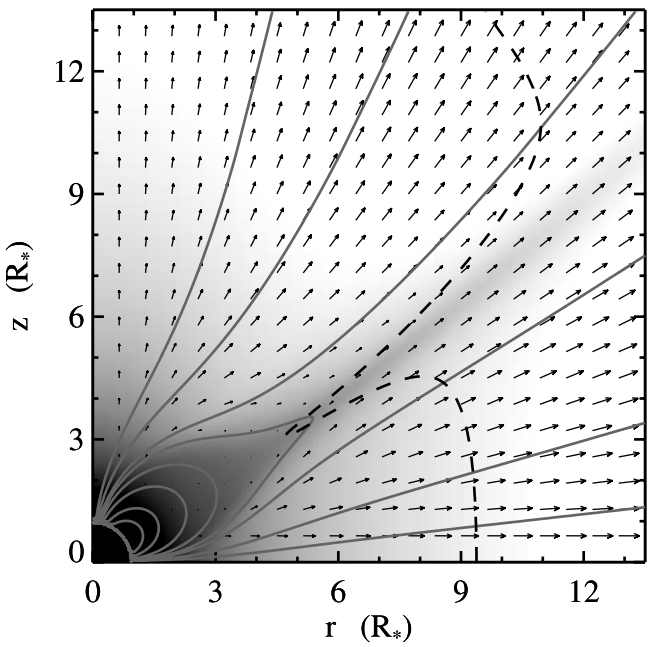

FIG. 4.—Same as Fig. 1, but for the 2 kG quadrupole case. The maximum velocity vector corresponds to 170 km s^{-1}.

fields than we consider here. To begin to quantify the effects of higher order fields, we ran two cases that were initialized with a quadrupolar field of the form

$$B_R = B_*\left(3\cos^2\theta - 1\right)\left(\frac{R_*}{R}\right)^4$$
$$B_\theta = 2B_*\cos\theta\sin\theta\left(\frac{R_*}{R}\right)^4 \qquad (12)$$

in spherical coordinates.

We ran cases with B_* equal to 1 and 2 kG, listed as "1 kG quad." and "2 kG quad.," respectively, in Table 2. Figure 4 illustrates the wind solution for the 2 kG quadrupole case. It is clear from the figure that, compared to the cases with a dipole field, the shape of Alfvén surface is quite different. Also, for a given value of B_*, the effective lever arm length is much shorter for the quadrupole case.

It is evident from Table 2 that the stellar wind torque from a star with a 200 G dipole field is comparable to that with a 1–2 kG quadrupole field. Thus, the stellar wind torque is very sensitive to surface field geometry. However, since the measured surface field strengths of ~2 kG likely include contributions from even higher multipoles than a quadrupole, it seems that the dipole component will generally dominate near the Alfvén surface. So the strength of the dipole component should generally be the most important for determining the torque.

4.2.4. *Mass-loss Rate*

We have thus far considered quite massive winds, motivated by recent suggestions in the literature for accretion-powered winds. However, the value of $\dot{M}_w$ is very uncertain and is likely to exhibit a wide range in values from one object to the next. In addition, it would be interesting to predict what torques may be expected for the winds from the nonaccreting, weak-line TTSs. We expect these stars to have solar-like winds that are quite enhanced relative to their main-sequence counterparts, yet probably less powerful than winds from the accreting stars.

Unfortunately, our method is limited to cases with lever arms that are not too long, since longer lever arms require a larger Alvén speed on the stellar surface. A large Alfvén speed increases the time for the simulation to run and increases the error in the solution (e.g., by increasing the effective diffusion rate in our code). For this practical reason, we were limited to running only two cases with lower $\dot{M}_w$ covering a range in $\dot{M}_w$ of a factor of 50. These are listed in the ninth and tenth rows of Table 2.

4.2.5. *Stellar Radius*

TTSs contract as they age, so stars of a given mass exhibit a range of radii during this phase. Thus, it is important to consider here different combinations of stellar mass and radius. Table 2 contains results from two cases with $R_* = 1.5\ R_\odot$ and $R_* = 3\ R_\odot$. Note that changing R_* changes $v_{\rm esc}$, so these cases have a different coronal temperature and Ω_*, in order that $c_s/v_{\rm esc}$ and f are constant. From the values in the table, it is evident that the stellar wind torque is very sensitive to R_*. The reason for this is twofold. First, since B_* is fixed, a larger stellar radius corresponds to a larger dipole moment ($\mu \equiv B_*R_*^3$), which is capable of conveying a larger torque. Second, a larger stellar radius decreases the surface gravity, and so the influence of the magnetic field relative to gravity is increased (i.e., $v_{\rm A}/v_{\rm esc}$ increases). Thus, $(r_{\rm A}/R_*)^2$ increases with R_*, and although Ω_* decreases (to keep f fixed), the quantity $\Omega_*R_*^2$ increases, so the net torque increases.

4.2.6. *Stellar Mass*

Cases with half and twice the fiducial stellar mass are also listed in Table 2. As with the cases of different R_*, note that changes in M_* change $v_{\rm esc}$, so we have adjusted the coronal temperature and Ω_* to keep the parameters listed in Table 1 fixed. As with the case of varying R_*, a change in $v_{\rm esc}$ changes the relative importance of the magnetic field with the gravity. Thus, $r_{\rm A}/R_*$ is larger for a smaller M_*. However, since we have fixed f, a smaller M_* means a smaller Ω_* so that the net stellar wind torque decreases.

4.2.7. *Wind Acceleration*

The increase of the wind speed with distance from the star depends on the details of the wind acceleration mechanism. In a Parker wind, the temperature (parameterized by $c_s/v_{\rm esc}$) and the cooling/heating of the gas as it flows (parameterized by γ) are the key physical properties determining the velocity profile in the wind. A hotter wind accelerates more rapidly and achieves a higher speed than a cooler wind. A wind with a larger γ (closer to 5/3) cools more rapidly as it expands, and so the bulk of the acceleration takes place closer to the star. Similarly, if the wind is instead accelerated by something other than thermal pressure, the velocity profile may be altered.

In order to quantify the effect of varying the acceleration in the wind, within the framework of the pressure-driving mechanism used here, we have run three more simulations. The results of these are listed in the last three rows of Table 2. In order, these represent winds that are hotter, colder, or with less heating (i.e., more adiabatic cooling) than the fiducial case. The relatively large effect of $c_s/v_{\rm esc}$ and γ on the wind speed near the stellar surface is evident by the very different values of ρ_* required to keep $\dot{M}_w$ fixed, listed in Table 2. The wind velocity at the base of the corona, for fixed $\dot{M}_w$, varies as the inverse of the variation in ρ_*. So these cases represent large differences in the wind acceleration rate. The effect on the torque is relatively small, but is not entirely negligible. It will be important for future work to determine the wind torques for different driving mechanisms. The preliminary conclusion to be drawn from this work is that the wind

velocity profile, and therefore wind driving mechanism, does not have a large effect on the torque.

5. SEMIANALYTIC FIT FOR THE EFFECTIVE ALFVÉN RADIUS

In § 2.1, we pointed out that no reliable formulation exists for predicting the Alfvén radius (and therefore torque) in a stellar wind from fundamental parameters. However our parameter study, even though somewhat limited, can be used to provide a numerically based approach to this question. We will use the results in future work, and it also will be of general interest for other stellar wind studies.

In a one-dimensional theory, one can assume that the magnetic field strength approximately follows a single power law of the form $B = B_*(R_*/R)^n$. Then the condition that the wind speed equals the Alfvén speed at r_A gives (e.g., Kawaler 1988; Tout & Pringle 1992)

$$\left(\frac{r_A}{R_*}\right)^{2n-2} = \frac{B_*^2 R_*^2}{\dot{M}_w v_{rA}}, \tag{13}$$

where v_{rA} is the wind speed at the Alfvén radius. There are a number of problems. First, the true magnetic field strength in a wind does not follow a single power law (e.g., Mestel & Spruit 1987). Second, the Alfvén surface is neither a sphere nor a cylinder and a spherical model is quite misleading. Third, and perhaps most vexing, is the fact that v_{rA} has different values at different points along the Alfvén surface and cannot be determined a priori. Finally, there is no explicit dependence of r_A on the spin rate or driving properties of the wind, which we also know to be false.

There is, however, a more general way of scaling the Alfvén radius that is suggested by basic theory. Another clue is that since the numerical simulations are carried out in normalized units, they are scalable to any system with similar characteristic speeds on the stellar surface (e.g., Matt & Balick 2004). This suggests that we can replace v_{rA} with the stellar surface escape speed and calculate the Alfvén radius using

$$\frac{r_A}{R_*} = K\left(\frac{B_*^2 R_*^2}{\dot{M}_w v_{esc}}\right)^m, \tag{14}$$

where K and m are dimensionless constants. The quantity inside the bracket measures the effective magnetization of the wind, is similar to that used by ud-Doula & Owocki (2002; see their eq. [7]), and arises naturally in disk wind theory (e.g., eq. [2.27] of Pelletier & Pudritz 1992). It is also a quantity that can be measured by observations of stellar properties and wind parameters.

In Figure 5, we plot r_A/R_* as a function of the quantity in brackets in equation (14) on a log-log scale, for all 17 of our simulations. Since we know equation (14) does not properly include the effects of stellar rotation or the wind driving mechanism, we calculate the best-fit K and m to the fiducial case and only those cases with variations on B_*, R_*, $\dot{M}_w$, and M_*. The fit, giving $K \approx 2.11$ and $m \approx 0.223$, is plotted as a line in the figure.

It is remarkable that this fit matches all of the relevant simulations (filled circle and diamonds in the figure) with an error of less than 1%. This is at the level of precision of the numerical method (Matt & Balick 2004). Remember that we have taken c_s/v_{esc} and f as our parameters, so that cases with a different value of v_{esc} (i.e., those with different R_* and M_*) actually also have different wind temperatures (i.e., c_s) and stellar angular spin rates

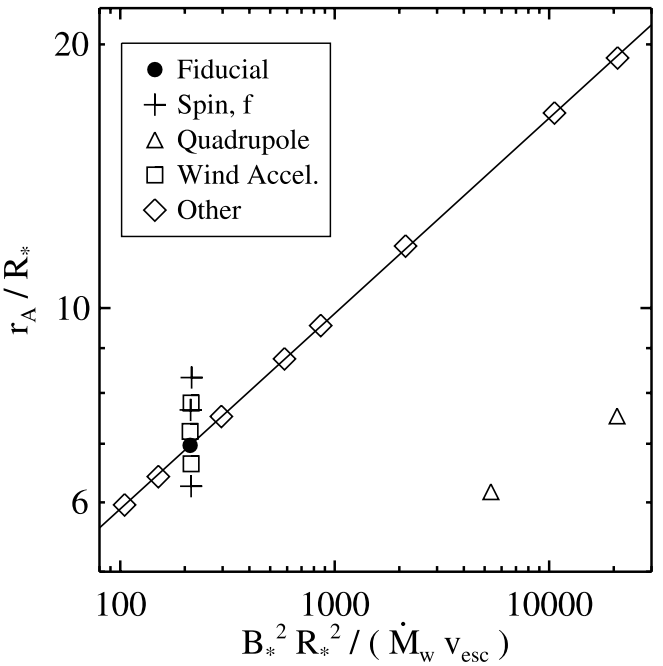

FIG. 5.—Effective lever arm length in the stellar wind vs. the quantity in brackets in eq. (14). Shown are the results of our entire parameter study including the fiducial case (*filled circle*); cases with different spin rates (*plus signs*); cases with a quadrupole field (*triangles*); cases with different c_s/v_{esc} or γ (*squares*); and all other cases (*diamonds*), representing those with different values of B_*, R_*, $\dot{M}_w$, or M_*. The line represents the best fit to the fiducial and "other" cases, given by eq. (14) with $K \approx 2.11$ and $m \approx 0.223$.

(Ω_*) than the fiducial case. If we had chosen Ω_* and c_s as our fixed parameters, there would be a lot more scatter of the diamonds around the line in Figure 5. Furthermore, our simulations self-consistently capture the interaction between the stellar wind, magnetic field, and rotation, without resorting to assumptions about (for example) the extent of the dead zone, the dependence of magnetic field strength with radius, or latitudinal variations in wind quantities. Therefore, our semianalytic formulation appears to be an improvement over existing theory.

Equation (14) does have some limitations. Neither the previous analytic formulations nor our own semianalytic approach properly include the effects of varying stellar rotation or wind driving (as evident in Fig. 5). As an illustrative example, in a smaller parameter study with a rotation rate comparable to the solar rate (not presented here), we found that $K \approx 3.0$ and $m \approx 0.19$. In addition, note that a line connecting the two points with a quadrupole field suggests $K \approx 1.7$ and $m \approx 0.15$ for these cases. Thus, the indices K and m are quite sensitive to the field geometry and have a smaller (but non-negligible) sensitivity to changes in the stellar spin rate and the wind acceleration rate/mechanism. We leave the precise determination of the sensitivity of r_A to these parameters for future work.

We can now combine equations (3) and (14) to get a formula for the stellar wind torque,

$$\tau_w = \frac{K^2}{\sqrt{2}} f v_{esc}^{1-2m} \dot{M}_w^{1-2m} R_*^{1+4m} B_*^{4m}, \tag{15}$$

although we know this does not properly contain the dependence (for example) on f. This equation is essentially the same as that derived by Kawaler (1988), except for the value of the dimensionless constant out front and of the expected value of the exponent

parameter m. The constant is not so crucial, and usually this can be calibrated to the solar wind torque for a predictive theory (although we have not done this here). On the other hand, the value of m is of far greater importance for predicting the torque for a range of parameters.

In particular, authors typically have chosen a power law such that the stellar wind torque is nearly or completely independent of $\dot{M}_w$ (effectively, $m = 0.5$), which results in $\tau_w \propto B_*^2$ (e.g., Kawaler 1988; Pinsonneault et al. 1989; Barnes & Sofia 1996; Bouvier et al. 1997). Our basic understanding of the observed Skumanich-style (Skumanich 1972) spin-down of main-sequence stars ($\Omega_* \propto t^{-1/2}$), as well as the expected dependence of magnetic field strength with rotation rate (Belcher & MacGregor 1976), appears to rely on this or a similar formulation. Our fit value of $m \approx 0.223$ gives approximately $\tau_w \propto B_*^{0.9}$ (this was also found by Washimi & Shibata 1993), which is substantially different.

In order to understand the difference between our value of the exponent and that used by others, it is instructive to consider the power-law formulation of the magnetic field used to derive equation (13). It is generally expected (e.g., Mestel 1984; Mestel & Spruit 1987; Kawaler 1988) that when the surface magnetic field is dipolar, as we are considering here, the effective power-law index of the magnetic field in the flow will lie somewhere between the value for a dipole ($n = 3$) and that for a split monopole ($n = 2$). This has been the primary justification for the power laws used in the literature. Indeed, our simulations display the expected behavior of exhibiting a dipolar geometry near the star and an approximately monopolar geometry far from the star (e.g., Fig. 1). However, by comparing equations (13) and (14) we see that our fit value of $m \approx 0.223$ seems to imply a magnetic power law of $n \approx 3.2$.

It is important to realize that the divergence of the magnetic field in the flow, captured by the power-law index n, is not the only important effect, and this is why the formulation of equation (13) is misleading. Here are two specific reasons: First, using one-dimensional reasoning, in an accelerating wind, the behavior of $v_{r\mathrm{A}}$ mitigates the response of r_A to the parameters. For example, for an increase in B_*, the Alfvén radius will become larger, but since the flow is accelerating, $v_{r\mathrm{A}}$ will also increase. Kawaler (1988) made the approximation that $v_{r\mathrm{A}}$ equals the escape speed at r_A. In this case, $v_{r\mathrm{A}}$ *decreases* with radius, giving the opposite effect of an accelerating wind. Similarly, the approximations of Mestel (1984) that $v_{r\mathrm{A}}$ is constant for a slow rotator and proportional to $\Omega_* r_\mathrm{A}$ for a fast rotator do not well approximate the acceleration exhibited in the winds we simulated. The second reason for the surprisingly weak dependence of r_A on parameters is in the amount of open magnetic flux that participates in the flow, which again is not included in the derivation of equation (13), and which again mitigates the effect of parameters on r_A. For example, for an increase in B_*, a smaller area on the stellar surface will have open flux (e.g., compare Figs. 1 and 3, and see Mestel & Spruit 1987), so r_A will not increase as much as expected in the magnetic power-law formulation.

In future work, it will be important to extend equation (14) to include the effects of rotation, etc. Furthermore, much work is needed to explore the full consequences (e.g., for main-sequence stars) of the significantly smaller exponent we find, compared to many previous works.

6. SUMMARY AND CONCLUSIONS

Using two-dimensional (axisymmetric) MHD simulations, we computed steady state, stellar wind solutions for a parameter range appropriate for TTSs. We carried out a parameter study including variations of the stellar mass, radius, surface magnetic field strength, and rotation rate, as well as mass-loss rate, wind acceleration rate, and two different magnetic geometries (dipole and quadrupole). Our solutions enabled us to determine the angular momentum carried in the wind, and its dependence on many of the parameters of the system. Our main conclusions can be summarized as follows.

1. For fiducial parameters, the torque is of the same order ($\sim 10^{36}$ erg) as estimated in Paper I. Therefore, if the stellar winds of TTSs have similar parameters to those considered here, they should have a significant influence on the stellar spin.

2. The stellar winds are in the regime of moderately fast magnetic rotator winds. They produce jets, as well as a wide-angle flow (see, e.g., Matt & Balick 2004), which should interact with, and be modified by, surrounding material (not included in our simulations; e.g., Gardiner et al. 2003; Shang et al. 2006).

3. The cases with quadrupole fields resulted in a torque that is much weaker than cases with a dipole field of the same surface field strength. Specifically, we find that a 200 G dipole field exerts the same stellar wind torque on a star as a 1–2 kG quadrupole. This illustrates the very strong effect of magnetic geometry on the stellar wind torque.

4. We ran cases where the mass-loss rate and other parameters were fixed, but the thermal wind driving parameters were varied. For large variations in the wind acceleration, the torque changed by less than a factor of 2. This suggests that the details of the velocity profile are not of fundamental importance, and our solutions should be a reasonable approximation for winds with other wind driving mechanisms. However, it will still be important for future work to compare our torque results to stellar wind solutions that use alternative driving mechanisms.

5. Our determination of the torque allowed us to calculate the Alfvén radius (via eq. [3]), which is a fundamental quantity in MHD wind theory. We compared our numerical solutions to previous analytic work and obtained a semianalytic formulation for $r_\mathrm{A}/R_* \propto [B_*^2 R_*^2/(\dot{M}_w v_\mathrm{esc})]^m$, with $m \approx 0.22$ (eq. [14]), that well describes many of our simulations with dipole fields. This formulation appears to be an improvement over existing work, and the exponent m is significantly smaller than usually assumed.

We will continue to develop the theory of accretion-powered stellar winds in forthcoming work. In a companion paper (the third in this series; Matt & Pudritz 2008b), we compare the stellar wind torques computed here to the torques expected to arise from the interaction between the star and an accretion disk. We find spin-equilibrium (net zero torque) solutions and test the suggestion of Paper I. In a later paper, we will use the stellar wind solutions of this work to compute emission properties of TTS coronal winds.

Initial results of various aspects of this work were presented at a number of meetings, and we wish to thank many participants who provided interesting questions, discussion, and ideas, including Gibor Basri, Sylvie Cabrit, Steve Cranmer, Andrea Dupree, Suzan Edwards, Christian Fendt, Will Fischer, Shu-ichiro Inutsuka, Chris Johns-Krull, Marina Romanova, Frank Shu, Keivan Stassun, Asif ud-Doula, Jeff Valenti, and others. We also thank the referee, Ruben Krasnopolsky, for his useful suggestions for improving the paper, and KITP for hospitality and support (NSF grant PHY05-51164) while we finished this manuscript. S. M. is supported by the University of Virginia through a Levinson/VITA Fellowship partially funded by the Frank Levinson Family Foundation through the Peninsula Community Foundation. R. E. P. is supported by a grant from NSERC.

REFERENCES

Anderson, J. M., Li, Z., Krasnopolsky, R., & Blandford, R. D. 2003, ApJ, 590, L107
Bacciotti, F., Ray, T. P., Mundt, R., Eislöffel, J., & Solf, J. 2002, ApJ, 576, 222
Barnes, S. A. 2003, ApJ, 586, 464
Barnes, S., & Sofia, S. 1996, ApJ, 462, 746
Belcher, J. W., & MacGregor, K. B. 1976, ApJ, 210, 498
Bisnovatyi-Kogan, G. S., & Lamzin, S. A. 1977, Soviet Astron., 21, 720
Bogovalov, S., & Tsinganos, K. 2001, MNRAS, 325, 249
Bouvier, J., Alencar, S. H. P., Harries, T. J., Johns-Krull, C. M., & Romanova, M. M. 2007, in Protostars and Planets V, ed. B. Reipurth, D. Jewitt, & K. Keil (Tucson: Univ. Arizona Press), 479
Bouvier, J., Forestini, M., & Allain, S. 1997, A&A, 326, 1023
Cieza, L., & Baliber, N. 2007, ApJ, 671, 605
Coffey, D., Bacciotti, F., Ray, T. P., Eislöffel, J., & Woitas, J. 2007, ApJ, 663, 350
Coffey, D., Bacciotti, F., Woitas, J., Ray, T. P., & Eislöffel, J. 2004, ApJ, 604, 758
Cranmer, S. R., van Ballegooijen, A. A., & Edgar, R. J. 2007, ApJS, 171, 520
Decampli, W. M. 1981, ApJ, 244, 124
Dupree, A. K., Brickhouse, N. S., Smith, G. H., & Strader, J. 2005, ApJ, 625, L131
Edwards, S., Fischer, W., Hillenbrand, L., & Kwan, J. 2006, ApJ, 646, 319
Edwards, S., Fischer, W., Kwan, J., Hillenbrand, L., & Dupree, A. K. 2003, ApJ, 599, L41
Favata, F., Flaccomio, E., Reale, F., Micela, G., Sciortino, S., Shang, H., Stassun, K. G., & Feigelson, E. D. 2005, ApJS, 160, 469
Feigelson, E. D., & Montmerle, T. 1999, ARA&A, 37, 363
Feldman, W. C., Barraclough, B. L., Gosling, J. T., McComas, D. J., Riley, P., Goldstein, B. E., & Balogh, A. 1998, J. Geophys. Res., 103, 14547
Fendt, C., & Camenzind, M. 1996, A&A, 313, 591
Fendt, C., Camenzind, M., & Appl, S. 1995, A&A, 300, 791
Ferreira, J., Dougados, C., & Cabrit, S. 2006, A&A, 453, 785
Gardiner, T. A., Frank, A., & Hartmann, L. 2003, ApJ, 582, 269
Hartmann, L., Avrett, E., & Edwards, S. 1982, ApJ, 261, 279
Hartmann, L., Avrett, E. H., Loeser, R., & Calvet, N. 1990, ApJ, 349, 168
Hartmann, L., & MacGregor, K. B. 1980, ApJ, 242, 260
———. 1982, ApJ, 259, 180
Hartmann, L., & Stauffer, J. R. 1989, AJ, 97, 873
Herbst, W., Bailer-Jones, C. A. L., Mundt, R., Meisenheimer, K., & Wackermann, R. 2002, A&A, 396, 513
Herbst, W., Eislöffel, J., Mundt, R., & Scholz, A. 2007, in Protostars and Planets V, ed. B. Reipurth, D. Jewitt, & K. Keil (Tucson: Univ. Arizona Press), 297
Herbst, W., Rhode, K. L., Hillenbrand, L. A., & Curran, G. 2000, AJ, 119, 261
Holzer, T. E., Fla, T., & Leer, E. 1983, ApJ, 275, 808
Johns-Krull, C. M. 2007a, in Proc. IAU Symp. 243, Star-Disk Interaction in Young Stars, ed. J. Bouvier & I. Appenzeller (Cambridge: Cambridge Univ. Press), 31
———. 2007b, ApJ, 664, 975
Johns-Krull, C. M., & Gafford, A. D. 2002, ApJ, 573, 685
Johns-Krull, C. M., & Herczeg, G. J. 2007, ApJ, 655, 345
Johns-Krull, C. M., Valenti, J. A., Hatzes, A. P., & Kanaan, A. 1999, ApJ, 510, L41
Kawaler, S. D. 1988, ApJ, 333, 236
Keppens, R., & Goedbloed, J. P. 1999, A&A, 343, 251
———. 2000, ApJ, 530, 1036
Königl, A. 1991, ApJ, 370, L39
Königl, A., & Pudritz, R. E. 2000, in Protostars and Planets IV, ed. V. Mannings, A. P. Boss, & S. S. Russell (Tucson: Univ. Arizona Press), 759
Kraft, R. P. 1967, ApJ, 150, 551
Krasnopolsky, R. 2000, Ph.D. thesis, California Institute of Technology
Kurosawa, R., Harries, T. J., & Symington, N. H. 2006, MNRAS, 370, 580
Kwan, J., Edwards, S., & Fischer, W. 2007, ApJ, 657, 897
Li, J. 1999, MNRAS, 302, 203
MacGregor, K. B., & Brenner, M. 1991, ApJ, 376, 204
Matt, S., & Balick, B. 2004, ApJ, 615, 921
Matt, S., & Pudritz, R. E. 2005a, ApJ, 632, L135
———. 2005b, MNRAS, 356, 167
———. 2007, in Proc. IAU Symp. 243, Star-Disk Interaction in Young Stars, ed. J. Bouvier & I. Appenzeller (Cambridge: Cambridge Univ. Press), 299
———. 2008a, in Proc. 14th Cambridge Workshop on Cool Stars, Stellar Systems, and the Sun, in press (astro-ph/0701648)
———. 2008b, ApJ, in press
Mestel, L. 1968, MNRAS, 138, 359
———. 1984, in Proc. 3rd Cambridge Workshop on Cool Stars, Stellar Systems, and the Sun, ed. S. L. Baliunas & L. Hartmann (Berlin: Springer), 49
Mestel, L., & Spruit, H. C. 1987, MNRAS, 226, 57
Michel, F. C. 1969, ApJ, 158, 727
Okamoto, I. 1974, MNRAS, 166, 683
Paatz, G., & Camenzind, M. 1996, A&A, 308, 77
Parker, E. N. 1958, ApJ, 128, 664
Pelletier, G., & Pudritz, R. E. 1992, ApJ, 394, 117
Pinsonneault, M. H., Kawaler, S. D., Sofia, S., & Demarque, P. 1989, ApJ, 338, 424
Pneuman, G. W., & Kopp, R. A. 1971, Sol. Phys., 18, 258
Rebull, L. M., Wolff, S. C., & Strom, S. E. 2004, AJ, 127, 1029
Rebull, L. M., Wolff, S. C., Strom, S. E., & Makidon, R. B. 2002, AJ, 124, 546
Reipurth, B., & Bally, J. 2001, ARA&A, 39, 403
Reipurth, B., Pedrosa, A., & Lago, M. T. V. T. 1996, A&AS, 120, 229
Richtmyer, R. D., & Morton, K. W. 1967, Difference Methods for Initial-Value Problems (2nd ed; New York: Wiley)
Sakurai, T. 1985, A&A, 152, 121
Sauty, C., Trussoni, E., & Tsinganos, K., 2002, A&A, 389, 1068
Schatzman, E. 1962, Ann. d'Astrophys., 25, 18
Shang, H., Allen, A., Li, Z.-Y., Liu, C.-F., Chou, M.-Y., & Anderson, J. 2006, ApJ, 649, 845
Shu, F., Najita, J., Ostriker, E., Wilkin, F., Ruden, S., & Lizano, S. 1994, ApJ, 429, 781
Skumanich, A. 1972, ApJ, 171, 565
Smirnov, D. A., Fabrika, S. N., Lamzin, S. A., & Valyavin, G. G. 2003a, A&A, 401, 1057
Smirnov, D. A., Lamzin, S. A., & Fabrika, S. N. 2003b, Astron. Lett., 29, 258
Smirnov, D. A., Lamzin, S. A., Fabrika, S. N., & Chuntonov, G. A. 2004, Astron. Lett., 30, 456
Soderblom, D. R. 1983, ApJS, 53, 1
Stassun, K. G., Ardila, D. R., Barsony, M., Basri, G., & Mathieu, R. D. 2004, AJ, 127, 3537
Stassun, K. G., Mathieu, R. D., Mazeh, T., & Vrba, F. J. 1999, AJ, 117, 2941
Stassun, K. G., Mathieu, R. D., Vrba, F. J., Mazeh, T., & Henden, A. 2001, AJ, 121, 1003
Suzuki, T. K. 2007, ApJ, 659, 1592
Suzuki, T. K., & Inutsuka, S.-i. 2006, J. Geophys. Res. Space Phys., 111, A06101
Tout, C. A., & Pringle, J. E. 1992, MNRAS, 256, 269
ud-Doula, A., & Owocki, S. P. 2002, ApJ, 576, 413
Vogel, S. N., & Kuhi, L. V. 1981, ApJ, 245, 960
Washimi, H., & Sakurai, T. 1993, Sol. Phys., 143, 173
Washimi, H., & Shibata, S. 1993, MNRAS, 262, 936
Weber, E. J., & Davis, L. J. 1967, ApJ, 148, 217
Yang, H., Johns-Krull, C. M., & Valenti, J. A. 2007, AJ, 133, 73